Research Square

Preprints are preliminary reports that have not undergone peer review.
They should not be considered conclusive, used to inform clinical practice,
or referenced by the media as validated information.

Evidence for Stepwise Oxetane Formation in an FeCl3 Catalyzed Carbonyl-Olefin Metathesis Reaction

Jennifer Hirschi

jhirschi@binghamton.edu

Binghamton University https://orcid.org/0000-0002-3470-0561

Tamal Das

Binghamton University https://orcid.org/0009-0002-0420-8178

Anuradha Dagar

Binghamton University

Chetan Joshi

Binghamton University

Madison Neukirch

Binghamton University

Mathew Vetticatt

Binghamton University https://orcid.org/0000-0001-5709-0885

Article

Keywords:

Posted Date: November 19th, 2026

DOI: https://doi.org/10.21203/rs.3.rs-11369390/v1

License: This work is licensed under a Creative Commons Attribution 4.0 International License.
Read Full License

Additional Declarations: There is **NO** Competing Interest.

Evidence for Stepwise Oxetane Formation in an $FeCl_3$ Catalyzed Carbonyl-Olefin Metathesis Reaction

Tamal Das[1,†], Anuradha Dagar[1,†], Chetan Joshi[1], Madison A. Neukirch[1], Mathew J. Vetticatt[1,*] & Jennifer S. Hirschi[1,*]

[1]Department of Chemistry, Binghamton University, Binghamton, New York 13902, USA.

[†]These authors contributed equally: Tamal Das, Anuradha Dagar.

[*]Corresponding authors: Jennifer S. Hirschi (jhirschi@binghamton.edu) and Mathew J. Vetticatt (vetticatt@binghamton.edu).

Abstract

Experimental ^{13}C kinetic isotope effects (KIEs) provide compelling qualitative evidence for a stepwise mechanism for oxetane formation in the intramolecular $FeCl_3$ catalyzed ring-closing carbonyl-olefin metathesis (COM) reaction forming polycyclic aromatic hydrocarbons. This finding is in stark contrast to the current mechanistic understanding of this reaction, where prior studies have proposed an asynchronous concerted [2+2] cycloaddition to be the operational mechanism for oxetane formation. Theoretical studies including AIMD simulations, predicted KIEs from density functional theory (DFT) studies, and quasiclassical direct dynamics trajectories provide quantitative validation for the stepwise pathway. Our computed free-energy profile reveals similar barrier heights for formation of the betaine intermediate and the subsequent ring-closure to form the oxetane intermediate resulting in both steps contributing to the observed KIEs. Calculations show that this stepwise mechanism is insensitive to the

substitution pattern on the olefin (2-methyl-1-propenyl versus styrenyl) and the nature of the carbonyl (ketone versus aldehyde) for COM reactions forming polycyclic aromatics.

Introduction

The carbonyl-olefin metathesis (COM) reaction is a valuable transformation that has garnered significant attention as a strategy for the synthesis of complex olefins.[1] The iron (III) chloride catalyzed intramolecular carbonyl-olefin metathesis reaction, pioneered by Schindler and co-workers, is arguably the most practical catalytic version of this important transformation (Fig. 1).[2] The mechanism of this reaction has been the subject of extensive scrutiny.[3] It is well established that the reaction proceeds via an oxetane intermediate, formed via cycloaddition between the carbonyl and the olefin moieties in the substrate. Subsequent cycloreversion delivers

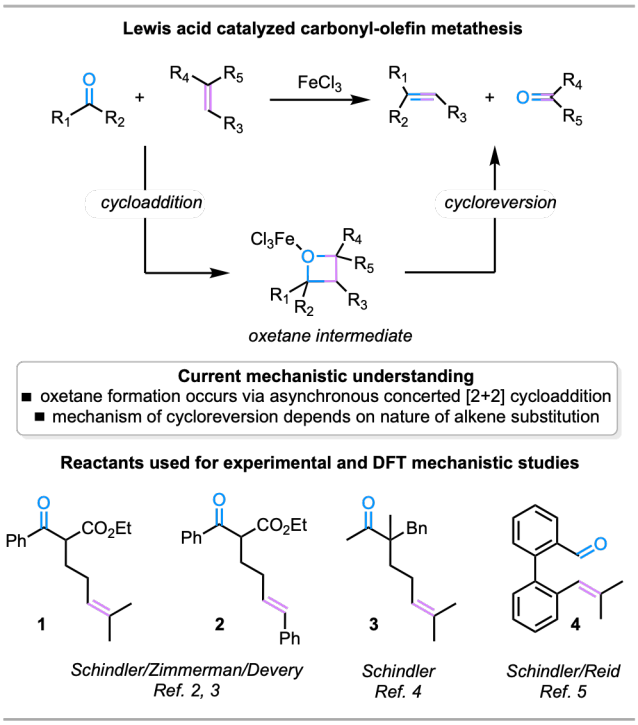


Fig. 1 | General scheme for the iron(III) chloride catalyzed carbonyl-olefin metathesis (COM) reaction and overview of mechanistic studies on intramolecular COM reactions performed by Schindler and co-workers.

the new olefin and a carbonyl by-product. Zimmerman, Devery, and Schindler have conducted detailed kinetic, spectroscopic, and computational studies to evaluate the mechanism using aryl ketone substrates such as **1** and **2**.[4] These studies led to the proposal of a concerted, asynchronous mechanism for oxetane formation for both **1** and **2**. The mechanism of the cycloreversion step was found to be dependent on the nature of the olefin – with prenyl substrate **1** proceeding via a concerted cycloreversion and styrenyl substrate **2** proceeding via a stepwise cycloreversion pathway. This mechanistic picture remains largely unchanged in subsequent studies with aliphatic ketone substrate **3**, though a dimeric $FeCl_3$ is invoked as the active catalyst in the reaction of **3**.[5] A concerted asynchronous cycloaddition mechanism for oxetane formation was also proposed by Reid and Schindler in the reaction of biaryl substrates such as **4** that yield polycyclic aromatic products.[6] Devery has explored catalyst speciation and has proposed the involvement of highly ligated octahedral Fe(III) complexes in this reaction;[7] however, these studies do not address the concerted versus stepwise nature of oxetane formation.

Overall, the consensus that has emerged from these studies is that $FeCl_3$ catalyzed COM proceeds via an asynchronous [2+2] cycloaddition transition state to form an intermediate oxetane, which then undergoes a concerted asynchronous or stepwise (depending on olefin substitution) cycloreversion step to yield the COM product. The Lewis acid ($FeCl_3$) is proposed to catalyze both key mechanistic events in the catalytic cycle. Intriguingly, this mechanistic picture stands in stark variance to other Lewis acid catalyzed COM reactions, in which stepwise mechanisms have been proposed for oxetane formation, even for substrates such as **1**.[8–11] This alternative mechanism for oxetane formation is initiated by carbon-carbon bond-formation between the Lewis acid activated carbonyl and the olefin resulting in a betaine intermediate, which then passes through a second ring-closing transition state to form the oxetane intermediate

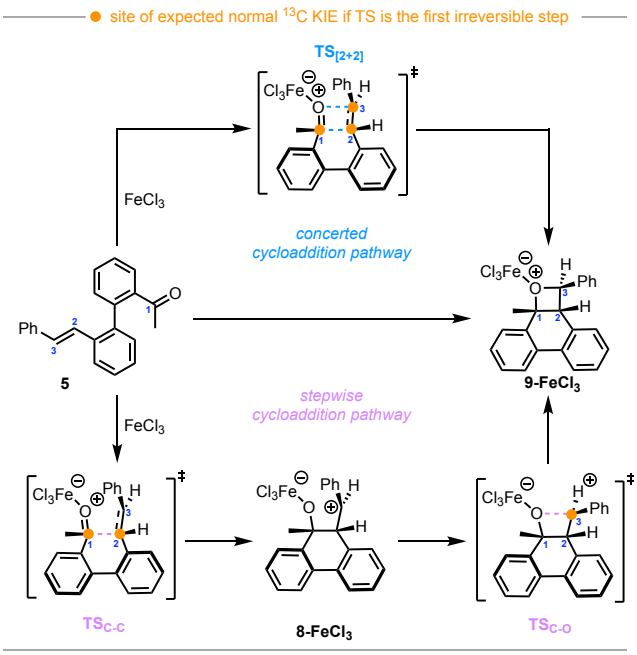


Fig. 2 | Key steps in the stepwise and concerted pathways for formation of key oxetane intermediate (9) in the ring-closing COM reaction of 5. Carbon atoms that would exhibit significant ^{13}C KIEs are highlighted in the relevant transition states.

(Fig. 2). Experimental characterization of the betaine intermediate is extremely challenging due to its fleeting existence. As a result, the proposed stepwise mechanism for oxetane formation in these systems is based primarily on DFT calculations. As such, experimental evidence for the concerted versus stepwise nature of the cycloaddition step that forms the key intermediate oxetane is lacking.

Considering the central importance of iron(III) chloride catalyzed COM reactions and the seemingly unique asynchronous concerted [2+2] transition state for oxetane formation proposed in several computational studies, we sought to obtain experimental evidence for the mechanism by which the key intermediate is formed. In a catalytic reaction, ^{13}C kinetic isotope effects (KIEs) determined at natural abundance report on the first irreversible step in the catalytic cycle for the reactant.[12] We envisioned that both the magnitude and location of ^{13}C KIEs would serve

as a sensitive probe to distinguish between a stepwise and concerted mechanism for the first irreversible step in the COM reaction.

Results

Experimental KIEs

The choice of experimental system is critical for probing the mechanism of oxetane formation using ^{13}C KIEs. Since ^{13}C KIEs at natural abundance report on the first irreversible step in a catalytic cycle, an ideal COM reaction is one in which oxetane formation is irreversible and the subsequent cycloreversion is facile. In an unpublished study (ref. 3), Schindler and Kwan utilized ^{13}C KIEs to evaluate the mechanism of oxetane formation for substrate **1**. A survey of the published computational studies on the $FeCl_3$ catalyzed COM reactions,[4,5] reveals that for substrates such as **1**–**3**, cycloreversion is turnover-limiting or co-turnover-limiting and would therefore be the major contributor to the observed KIEs. Thus, ^{13}C KIEs measured on a reactant such as **1** cannot unambiguously distinguish between stepwise and concerted oxetane formation (Supplementary Note 11 and Supplementary Figs. 14–16).

In 2017, Schindler and co-workers reported a ring-closing COM reaction of biaryl substrates such as **4** and **5** that delivers polycyclic aromatic hydrocarbons in good to excellent yields.[13] A subsequent computational study of this reaction by Schindler and Reid, using **4** as a model reactant, proposed that the reaction proceeds via an asynchronous concerted cycloaddition to form an oxetane intermediate, followed by a concerted cycloreversion step that lies 8 kcal/mol lower in energy than the first step (likely due to the gain in aromaticity as the polycyclic aromatic phenanthrene product is formed).[6] We recognized that this would be an ideal reaction to *experimentally* probe the mechanism of oxetane formation (*vide supra).* Thus, we chose the high-yielding ring-closing COM reaction of biaryl ketone **5** (reported 99% yield), bearing a

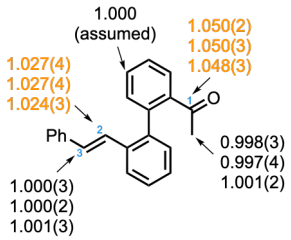


Fig. 3 | Experimental ^{13}C KIEs determined for the $FeCl_3$ catalyzed ring-closing COM reaction of 5. The three sets of numbers represent independent experiments and the numbers in parenthesis are the standard deviation in the last digit as determined from six measurements.

styrenyl alkene, as the model system for our ^{13}C KIE study to probe the mechanism of oxetane formation.[13]

The two possible mechanisms for oxetane formation from **5** are shown in Fig. 2. The sites of the expected normal ^{13}C KIEs for each mechanism are indicated in orange highlights. If the first irreversible step involves a concerted asynchronous [2+2] transition state ($\mathbf{TS_{2+2}}$) for oxetane formation – a normal ^{13}C KIE would be expected on all three carbon atoms C1, C2, and C3. On the other hand, if oxetane formation occurs via a stepwise mechanism with irreversible formation of a betaine intermediate (**8**) via $\mathbf{TS_{C\text{-}C}}$ (Fig. 2), this would result in significant normal ^{13}C KIEs on only C1 and C2 (not C3). Finally, if the reaction proceeds via a stepwise pathway with reversible formation of **8** followed by irreversible formation of oxetane (**9**) via $\mathbf{TS_{C\text{-}O}}$ (Fig. 2), a normal ^{13}C KIE will be observed only on C3, as this is the only center that is undergoing a bonding change at this TS.

The $FeCl_3$ catalyzed COM reaction of **5** in dichloroethane at room temperature was taken to ~75 % conversion and the unreacted **5** was reisolated from the reaction mixture. The ^{13}C isotopic composition of the recovered **5** was compared to a sample of **5** that was not subjected to reaction using quantitative NMR methodology. From the relative isotopic composition and the fractional conversions, ^{13}C KIEs for **5** were determined in a standard way (Supplementary Note 3, Supplementary Figs. 1–3 and Supplementary Table 1). The results from this experiment,

performed in triplicate, are shown in Fig. 3. The key result is the observation of a significant normal ^{13}C KIE on the carbonyl carbon (C1) and on one of the olefin carbon atoms (C2). Notably, there is no significant KIE on the other olefin carbon (C3). The qualitative interpretation of the experimental KIEs is that only C1 and C2 are involved in the first irreversible step in the catalytic cycle – a scenario that is *inconsistent* with a concerted mechanism (**TS_{2+2}**) being the first irreversible step in the catalytic cycle (*vide supra*). Importantly, the experimental KIEs are qualitatively consistent with a stepwise mechanism for oxetane formation proceeding via irreversible (and likely turnover-limiting) **$TS_{C\text{-}C}$**. However, a theoretical analysis of the reaction coordinate is necessary to understand the mechanistic details of this reaction and to further validate the interpretation of the experimental ^{13}C KIEs.

AIMD simulations

To address the question of whether the reaction proceeds via concerted or stepwise cycloaddition in the presence of solvent, we performed Born–Oppenheimer *ab initio* molecular dynamics (AIMD) simulations using the QUICKSTEP module of the CP2K 7.1 package.[14] The solvent-solute structure was modeled using a cubic periodic cell of dimensions 25.0 Å × 25.0 Å × 25.0 Å containing complex **5-$FeCl_3$** solvated with 50 dichloroethane (DCE) molecules. Atomic forces were estimated using density functional theory (DFT) calculations with the Perdew−Burke−Ernzerhof (PBE) exchange-correlation functional.[15] We applied a pure functional over a hybrid functional (e.g. B3LYP) to avoid the computational cost for this large system. The Kohn−Sham orbitals were described with hybrid Gaussian/plane-wave basis functions – a DZVP basis set and Goedecker−Teter−Hutter (GTH) pseudopotential were employed for all atoms.[16] The auxiliary plane-wave basis set was expanded up to a 280 Ry cutoff. The Grimme D3 dispersion correction was used to describe dispersion forces.[17] With this

129 method for performing AIMD simulations, we employed a metadynamics approach at 298 K for
130 enhanced sampling of the conformational space or rare events to understand the reaction
131 mechanism and to obtain the free energy profile for oxetane formation in the $FeCl_3$-catalyzed
132 COM reaction of **5**. (full details of this method are included in Supplementary Notes 6–8 and
133 Supplementary Movie 1) Such an approach is used to interrogate the nature of transition states,
134 the effect of solvent stabilization, the timing of bond formation or cleavage, and the stability and
135 lifetime of the intermediate species.[18–20]

136 We used coordination numbers (CNs), given by $CN = [1 - (d/d_0)^6]/ [1 - (d/d_0)^{12}]$, where d
137 is the distance between two atoms and d_0 is a reference distance, as collective variables (CVs).
138 The first collective variable, CV1, follows the bond formation between the carbonyl carbon (C1)
139 and one of the carbon atoms of the olefin (C2). The second collective variable, CV2, follows the
140 bond formation between the carbonyl oxygen and the other carbon atom of the olefin (C3). The
141 reference distances (d_0) corresponding to CV1 and CV2 are 2.8 Å and 3.0 Å, respectively. The
142 starting point for the metadynamics simulation was determined by equilibrating **5-$FeCl_3$** in the
143 DCE solvent box for 3 ps while maintaining constraints on the key bond-forming centers (C1,
144 C2, C3, and O) during the simulation. After this initial equilibration, we introduced a bias
145 potential on the coordination number following the formation of C1−C2 and C3−O bonds (the
146 collective variables (Fig. 4). This bias potential was added gradually to allow the entire free
147 energy surface (FES), including the transition states and the different intermediate regions, to be
148 sampled during the simulation. This enhanced sampling method allows for exploration of the
149 carbonyl-olefin metathesis reaction pathways without prior knowledge of the FES landscape.

150 The FES that connects the reactant (**5-$FeCl_3$**) and the oxetane intermediate (**9-$FeCl_3$**)
151 obtained using this procedure is shown in Fig. 4A (see also Supplementary Figs. 7 and 8). The

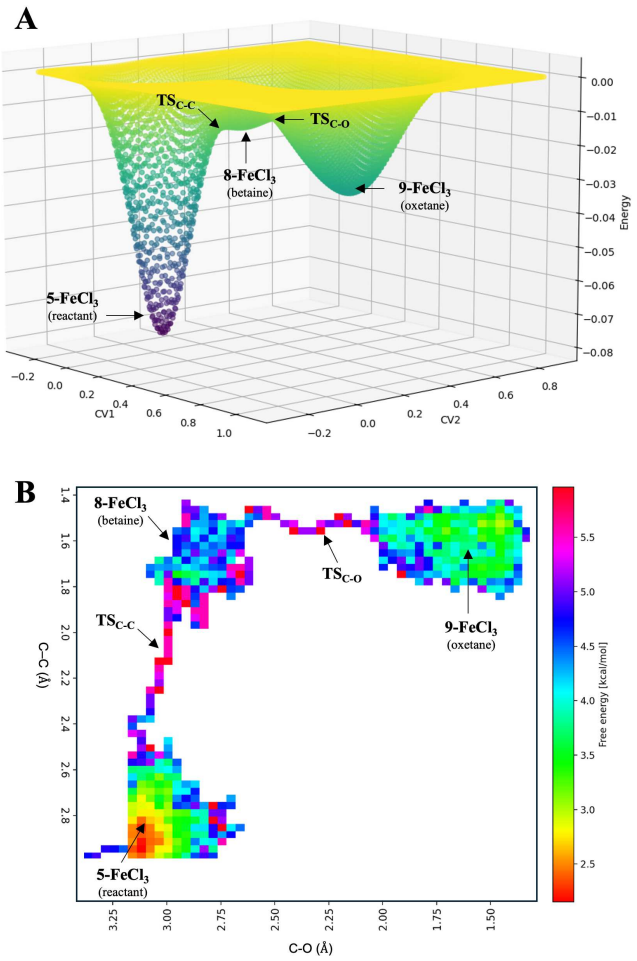


Fig. 4 | *Ab initio* metadynamics free energy surface for oxetane formation from 5-FeCl$_3$. (A) 3D free energy surface using *ab initio* metadynamics simulation of carbonyl-olefin metathesis reaction in a cubic box of 50 DCE solvent molecules. **(B)** Free energy surface starting from the reaction complex (**5-FeCl$_3$**) traverses through the metastable betaine intermediate via C-C bond formation and then C-O bond formation to make the four-membered stable oxetane intermediate.

first observation is that in the path that connects these two minima on the FES, there is a metastable betaine intermediate (**8-FeCl$_3$**) that resides in a shallow energy well between two saddle points (**TS$_{C-C}$** and **TS$_{C-O}$**) that correspond to two distinct bond-forming events – carbon-carbon bond-formation via **TS$_{C-C}$** followed by carbon-oxygen bond-formation via **TS$_{C-O}$**. Fig. 4B is a 2D representation of the minimum energy path (MEP) on the FES and indicates the timescale and relative stability of the reactants and intermediates in the metadynamics simulation. This analysis shows that after passing through the region of **TS$_{C-C}$**, the charge-

separated **8-$FeCl_3$** has a lifetime of about 2 ps before proceeding to **9-$FeCl_3$** via **$TS_{C\text{-}O}$**. The orange and green areas of Fig. 4B correspond to the lowest (**5-$FeCl_3$**) and second lowest (**9-$FeCl_3$**) minima on the FES, respectively while the bluish-green area of Fig. 4B corresponds to the metastable betaine intermediate **8-$FeCl_3$**. If this reaction proceeded through a concerted asynchronous [2+2] transition state as originally proposed, the two minima would have been connected by a single saddle point (**TS_{2+2}**) with the absence of a long-lived intermediate species (trajectories would cross from **5-$FeCl_3$** to **9-$FeCl_3$** without spending considerable time in the **8-$FeCl_3$** intermediate region). Identical results were obtained when we performed these AIMD simulations in the absence of explicit solvent molecules suggesting that the existence of the intermediate is not an artifact of the computational method and that inclusion of solvent is not necessary to locate the metastable betaine intermediate (Supplementary Fig. 9). This is also supported by static DFT calculations and quasiclassical dynamics trajectories (*vide infra*).

Analysis of the relative energies of the two saddle points on the FES (AIMD using PBE-D3/DZVP-GTH) reveals that $TS_{C\text{-}O}$ is 0.8 kcal/mol higher in free energy than $TS_{C\text{-}C}$. Considering that the AIMD simulations utilize relatively inexpensive methods to reduce computational cost (*vide supra*), the next step in our study was to evaluate the entire free energy profile of the reaction using several high-level DFT methods. The purpose of this approach was to – (a) to evaluate the relative energies of **$TS_{C\text{-}C}$** and **$TS_{C\text{-}O}$** in order to identify the first irreversible step in the catalytic cycle that determines the magnitude of the experimental ^{13}C KIEs, and (b) to predict KIEs for the relevant TSs for a quantitative interpretation of the experimental KIE values.

DFT analysis of the reaction coordinate

We initially modeled the cycloaddition and cycloreversion steps in the COM reaction of **5** catalyzed by $FeCl_3$ using B3LYP-D3(BJ)/6-31+G* and a CPCM[21,22] solvent for dichloroethane

as executed in Gaussian 16.[23] Intrinsic reaction coordinate (IRC) calculations were performed to connect the transition states to the minima in both the forward and reverse directions. The Gibbs free energies reported herein are the qRRHO-corrected free energies at room temperature.[24,25] For comparison with our experimental KIEs, we predicted ^{13}C KIEs for each of the TSs from the scaled vibrational frequencies using the Bigeleisen-Mayer equation as implemented in PyQuiver.[26–28] A Wigner tunneling correction was applied to the predictions (Supplementary Notes 4 and 5, Supplementary Fig. 4 and Supplementary Tables 3–5).[29]

The results from this initial DFT evaluation of the reaction coordinate are shown in Fig. 5. The reaction is initiated by the coordination of the Lewis acid to the carbonyl oxygen of **5** to form the complex **5**–$\mathbf{FeCl_3}$. The activated ketone undergoes carbon-carbon bond-formation ($\mathbf{TS_{C\text{-}C}}$) to form a charge-separated betaine intermediate **8**–$\mathbf{FeCl_3}$. This step has a barrier of 15.5 kcal/mol relative to **5**–$\mathbf{FeCl_3}$.The intermediate **8**–$\mathbf{FeCl_3}$ undergoes the C-O bond-forming step via $\mathbf{TS_{C\text{-}O}}$, which has a free energy barrier of 14.2 kcal/mol and leads to the formation of oxetane intermediate **9**–$\mathbf{FeCl_3}$. As expected, the cycloreversion from **9**–$\mathbf{FeCl_3}$ proceeds via a concerted asynchronous retro [2+2] transition state with a low energy barrier of only 11.4 kcal/mol.

The ^{13}C KIE predictions for each of the three TSs are shown in Fig. 5B. Comparison of experimental and predicted KIEs for $\mathbf{TS_{C\text{-}C}}$ indicates that while the predicted KIEs at C1 and C3 are in excellent agreement with experiment, C2 is significantly over-predicted for this TS (predicted value of 1.039 versus experimental of 1.026). As shown in Fig. 5B, the experimental and predicted matches for the KIEs are in poor agreement with a scenario that attributes the expression of the KIE to $\mathbf{TS_{C\text{-}O}}$ or $\mathbf{TS_{Rev}}$ as the sole irreversible step in the catalytic cycle. However, since $\mathbf{TS_{C\text{-}O}}$ is 1.3 kcal/mol lower in energy than $\mathbf{TS_{C\text{-}C}}$, ~89% of the observed KIEs should come from $\mathbf{TS_{C\text{-}C}}$ while ~11% should be attributed to $\mathbf{TS_{C\text{-}O}}$. Accordingly, we calculated

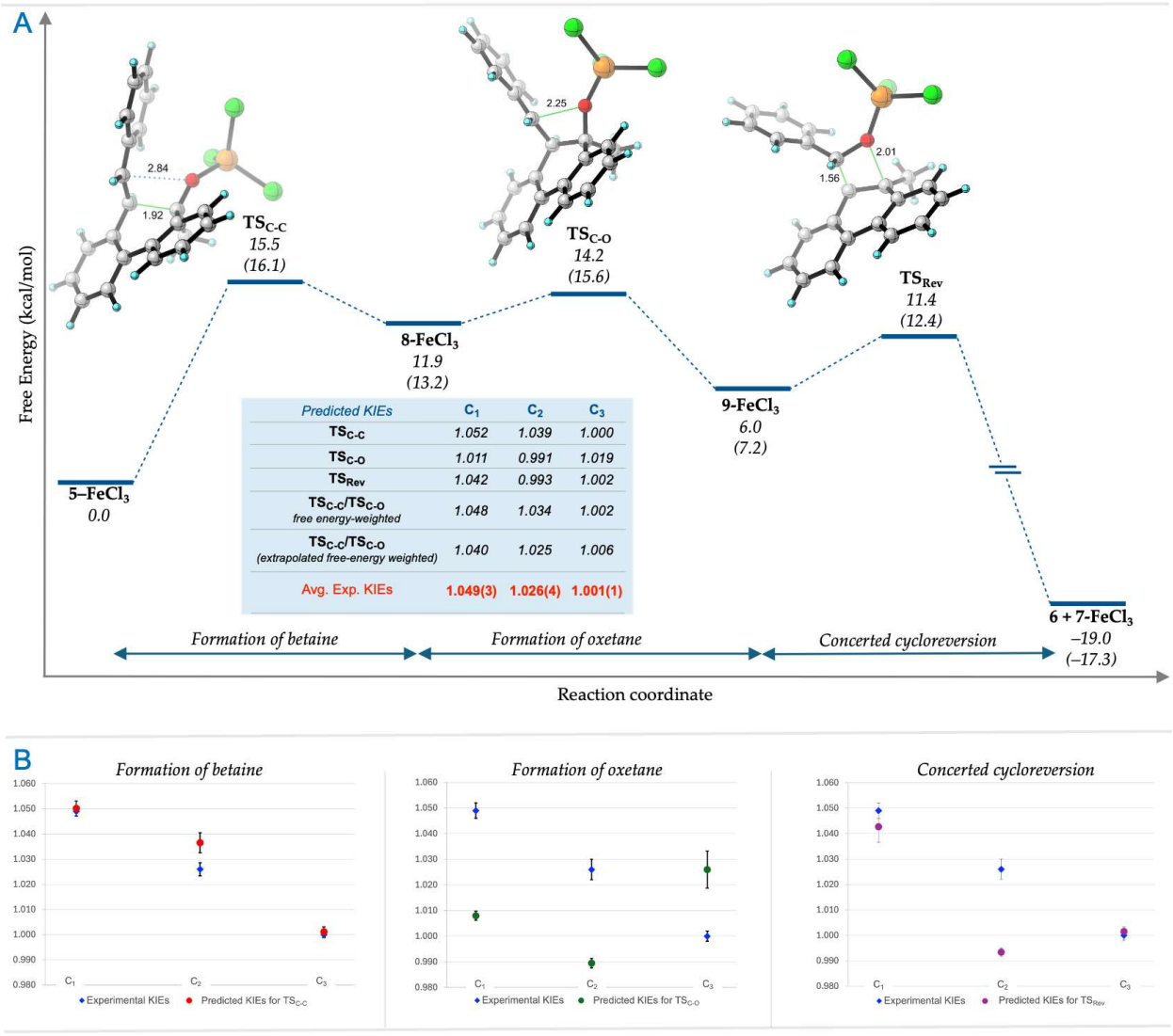


Fig. 5 | Free energy profile and predicted ^{13}C KIEs for the FeCl$_3$ catalyzed ring-closing COM of 5. **(A)** Free energy profile for FeCl$_3$ catalyzed ring-closing COM of **5** calculated at B3LYP-D3(BJ)/6-31+G* CPCM (dichloroethane) level of theory along with a comparison of experimental and predicted KIEs. Extrapolated free-energies computed from single-point energy calculations at B3LYP-D3(BJ)/6-311++G** CPCM (dichloroethane) are shown in parenthesis. **(B)** Comparison of experimental KIEs with the average predicted KIEs at C1, C2, and C3 for the three key TSs along the reaction coordinate. The error bars on the predicted KIEs are from computations performed using 6 different DFT methods.

the free energy-weighted KIEs based on these contributions from the two TSs involved in stepwise oxetane formation (Fig. 5A) and found a slightly better agreement between predicted and experimental C2 KIEs (1.034 versus 1.026). We note here that this discrepancy does not change the general conclusion that oxetane formation is stepwise. Thus, *our experimental and*

*theoretical ^{13}C KIEs for the ring-closing COM reaction of **5** are consistent with a mechanistic scenario where oxetane formation occurs via a stepwise mechanism with both **$TS_{C\text{-}C}$** and **$TS_{C\text{-}O}$** contributing to the observed KIEs.*

Effect of DFT method, canonical variational transition state theory (CVTST) and quasiclassical direct dynamics

To test the functional dependence of the DFT energies and KIE predictions we modeled the full reaction coordinate using a total of six functionals – B3LYP-D3(BJ),[30] M06,[31] ωB97-xD,[32] M062X,[31] PBE-D3(BJ),[15] B97D[33] – all with a 6-31+G** basis set[34] (using the Karlsruhe family basis set def2-SVP,[35] the results do not change the conclusions of this section and the details are included in Supplementary Table 2) and a CPCM solvent model for dichloroethane. The energy-weighted ^{13}C KIEs and qRRHO-corrected free energies were then calculated for each DFT method as previously described (*vide supra*). The key findings from this expanded computational evaluation are detailed below.

Firstly, all DFT methods predict a stepwise mechanism for oxetane formation followed by a concerted cycloreversion TS (**TS_{Rev}**). Secondly, ***the predicted KIEs for all TSs displayed a general method independence, indicating that the key geometric features of the transition structures did not vary significantly based on the choice of DFT method*** (see error bars of the predicted KIEs in Fig. 5B). For example, the average predicted KIE from the six DFT methods at C1, C2, and C3 for **$TS_{C\text{-}C}$** are 1.050 ± 0.002, 1.037 ± 0.003, and 1.001 ± 0.001 respectively (Fig. 5B and Supplementary Table 3). A comparison of the average experimental and predicted KIEs with the corresponding error bars for all three TSs illustrates that **$TS_{C\text{-}C}$** gives the best match to the experimental KIEs even though the average C2 KIE is over-predicted (Fig. 5B). Finally, the free energy profile for five out of the six DFT methods are qualitatively consistent with the

Table 1 | Energy-weighted KIE predictions obtained from seven DFT methods based on the relative free energy of the two TSs involved in oxetane formation.

DFT method	$\Delta\Delta G^{\ddagger}$(kcal/mol) ($TS_{C\text{-}C} - TS_{C\text{-}O}$)	Free energy-weighted predicted KIEs		
		C_1	C_2	C_3
B3LYP-D3(BJ)/6-31+G* CPCM	+1.25	1.048	1.034	1.002
B3LYP-D3(BJ)/6-31+G** CPCM	+1.17	1.047	1.033	1.002
B3LYP-D3(BJ)/6-311++G** CPCM	+0.85	1.044	1.030	1.004
M06/6-31+G** CPCM	+1.36	1.044	1.028	1.004
ωB97XD/6-31+G** CPCM	+3.49	1.051	1.036	1.002
M062X/6-31+G** CPCM	+0.23	1.032	1.018	1.016
PBE/6-31+G* CPCM	+0.49	1.036	1.022	1.006
B97D/6-31+G* CPCM	–1.90	1.010	0.992	1.019
Average experimental KIEs		1.049(3)	1.026(4)	1.001(1)

B3LYP-D3(BJ)/6-31+G* CPCM free energy surface shown in Fig. 5A – all methods exhibit a stepwise mechanism with $\mathbf{TS_{C\text{-}C}}$ being higher in energy than $\mathbf{TS_{C\text{-}O}}$ (the only outlier being B97D, see Table 1, Supplementary Note 12, Supplementary Figs. 5 and 6 and Supplementary Tables 9–22 for full details).

Based on the relative energies of $\mathbf{TS_{C\text{-}C}}$ and $\mathbf{TS_{C\text{-}O}}$, we calculated the energy-weighted KIEs for the DFT methods (Table 1). Comparison of the energy-weighted KIEs to experimental KIE values reveals that B3LYP-D3(BJ), M06, and ωB97-xD predictions are most closely aligned with the experimental values – this is due to all three of these functionals place $\mathbf{TS_{C\text{-}C}}$ between 0.85–3.49 kcal/mol higher in energy than $\mathbf{TS_{C\text{-}O}}$, resulting in larger contribution from $\mathbf{TS_{C\text{-}C}}$ to the predicted KIEs. In contrast, the energy-weighted KIEs from PBE-D3(BJ) and M062X underpredict the KIEs at C1 and C2 relative to the experiment since these functionals place $\mathbf{TS_{C\text{-}C}}$ 0.49 and 0.23 kcal/mol (respectively) above $\mathbf{TS_{C\text{-}O}}$. The resulting greater contribution of $\mathbf{TS_{C\text{-}O}}$ to the energy-weighted KIEs leads to an under-prediction of the KIE at C1/C2 and an over-prediction of the KIE at C3.

Finally, it was found that B97D was not a suitable method for computing the free energy surface of this reaction since it places $\mathbf{TS_{C\text{-}C}}$ 1.9 kcal/mol *below* $\mathbf{TS_{C\text{-}O}}$ resulting in predicted KIEs that are qualitatively and quantitatively inconsistent with experimental KIEs. This is likely

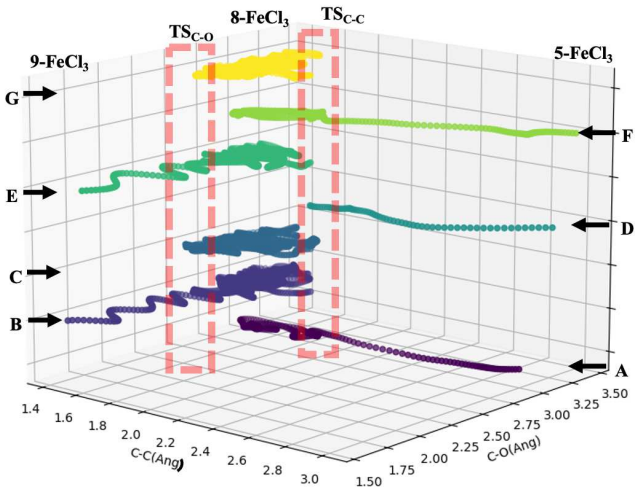
due to the absence of exact Hartree-Fock exchange contribution, which could affect the kinetic (barrier height)/thermochemical calculation.

Based on the comparison of experimental KIEs and theoretical energy-weighted KIEs we conclude that the free energy surfaces calculated using B3LYP-D3(BJ), ωB97-xD, and M06 are the most consistent with the actual free energy surface of the reaction and these functionals would be appropriate for future evaluation of similar systems. Thus, the key takeaways from the DFT study are that (a) the predicted KIEs for individual steps in the catalytic cycle are relatively insensitive to the DFT method (Fig. 5B), and (b) there is variability of the relative energies of the two TSs that contribute to the observed KIEs ($\Delta\Delta G^{\ddagger}$) (Table 1). This highlights the value of experimental measurements as a benchmark to computational mechanistic studies, especially when energy barriers lie relatively close in energy.

We performed canonical variational transition state (CVTS) calculations using POLYRATE17[36] to examine whether the saddle point on the free energy surface was significantly different from the potential energy saddle point (Supplementary Note 9 and Supplementary Figs. 10 and 11). The transition structure corresponding to the CVTS saddle point for betaine formation located on the B3LYP-D3(BJ)/6-31+G* CPCM (dichloroethane) energy surface has a C-C bond-forming distance of 1.87 Å and a C-O distance of 2.83 Å, which corresponds to a slightly "later" geometry than $\mathbf{TS_{C\text{-}C}}$ located using conventional TST. We also computed the ^{13}C KIE at C2 from the CVTS calculations including a small-curvature tunneling correction (SCT) and obtained a prediction of 1.042 – a value that is higher than the TST-Wigner KIE predictions of 1.039 (Supplementary Table 6). This result suggests that the discrepancy between the experimental and predicted KIE at C2 cannot be accounted for with the application

of the more advanced CVT-SCT treatment (see also Supplementary Table 7 and Supplementary Fig. 12).

As a final step in our theoretical interpretation of the experimental KIEs, we wanted to evaluate whether non-statistical recrossing plays a role in this stepwise mechanism for oxetane formation. Accordingly, quasiclassical downhill direct-dynamics trajectories[37,38] were initiated on the B3LYP-D3(BJ)/6-31+G* CPCM (dichloroethane) energy surface from the area of $\mathbf{TS_{C\text{-}C}}$ and were followed until either the betaine (or oxetane) was formed, or recrossing occurred to yield the pre-reactive complex **5-FeCl$_3$** (Supplementary Note 10, Supplementary Fig. 13, Supplementary Table 8 and Supplementary Movies 2 and 3). Some representative outcomes from the total of 118 trajectories that were obtained are shown in Fig. 6. The vast majority of the trajectories (92) remain in the area of the betaine intermediate (**8-FeCl$_3$**) after 500 fs (Fig. 6, C and G). When allowed to continue to about 2 ps, 11 of these trajectories traverse all the way to the oxetane intermediate **9-FeCl$_3$** (Fig. 6, B, and E). Therefore, we assume the 92 trajectories to be "productive". A significant number of trajectories (22) that fully form the C-C bond, traverse the area of **8-FeCl$_3$** for up to 250 fs, and then recross to form **5-FeCl$_3$** and are classified as 'deep recrossing' trajectories (Fig. 6, A and F). We use the ratio of "productive" and "deep recrossing" trajectories to weight the contributions of $\mathbf{TS_{C\text{-}C}}$ and $\mathbf{TS_{C\text{-}O}}$, respectively, to the observed KIEs. The small number of trajectories (4) that immediately recrossed (Fig. 6, D) were not included in the estimation of KIEs.[38] Since 19.3% (22/114) of the total trajectories underwent deep recrossing, we assume that for these trajectories, betaine formation is reversible, and $\mathbf{TS_{C\text{-}O}}$ contributes to the observed KIEs. On the other hand, for the 80.7% (92/114) of trajectories that either linger at **8-FeCl$_3$** or form product (**9-FeCl$_3$**), we assume that $\mathbf{TS_{C\text{-}C}}$ is irreversible and therefore accounts for the observed KIEs. The trajectory-weighted KIEs, shown in Fig. 6, give



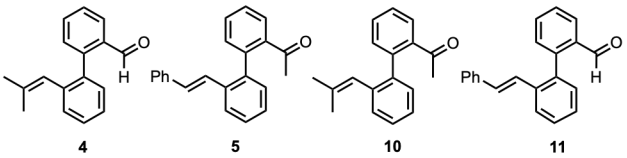
Predicted KIEs	C_1	C_2	C_3
TS_{C-C}/TS_{C-O} *trajectory recrossing weighted*	*1.044*	*1.029*	*1.003*
Avg. Exp. KIEs	**1.049(3)**	**1.026(4)**	**1.001(1)**

Fig. 6 | Stacked plots depicting C-C and C-O bond-formation in representative quasiclassical direct dynamics trajectories initiated from TS_{C-C} using B3LYP-D3(BJ)/6-31+G* CPCM (dichloroethane).

KIE predictions at C1 of 1.044, C2 of 1.029, and C3 of 1.003 and are all within 0.005 of the experimental measurements.

Effect of olefin and carbonyl substitution on the mechanism of oxetane formation

Reid and Schindler have proposed in ref. 6, using DFT calculations, a concerted mechanism for oxetane formation in the ring-closing COM reaction of **4**. This result is at variance with our proposed stepwise mechanism for oxetane formation for **5**. A closer inspection of the Schindler/Reid 'concerted' asynchronous TS for oxetane formation in the reaction of **4** revealed that the key bond distances in this TS are very similar to the corresponding distances in $\mathbf{TS_{C-O}}$ (Fig. 5A), the TS that converts betaine (**8-FeCl$_3$**) to oxetane (**9-FeCl$_3$**) in the stepwise mechanism for **5**. We were curious whether the nature of the carbonyl group (aldehyde in **4** versus ketone in **5**) or alkene substitution (2-methyl-1-propenyl in **4** versus styrenyl in **5**) would have an effect on the stepwise versus concerted nature of the mechanism for oxetane formation.



	$\Delta G^{\ddagger}$ (kcal/mol) relative to reactant-$FeCl_3$ complex for		
reactant	$TS_{C\text{-}C}$	$TS_{C\text{-}O}$	TS_{Rev}
4	8.6	13.2	6.0
5	15.5	14.2	11.4
10	13.1	14.3	7.1
11	12.3	13.6	11.4

Fig. 7 | Free energy barriers for key steps in the $FeCl_3$ catalyzed ring-closing COM reaction of four reactants with different combinations of substitution patterns at the carbonyl and the olefin moieties calculated at B3LYP-D3(BJ)/6-31+G* CPCM (dichloroethane) level of theory. The highest barrier step for each reactant is highlighted in red.

Accordingly, we explored the cycloaddition and cycloreversion steps in the ring-closing COM reaction of four different reactants (**4**, **5**, **10**, **11**) with combinations of either a methyl ketone or an aldehyde as the carbonyl component and either a styrenyl or 2-methyl-1-propenyl group as the olefin component using B3LYP-D3(BJ)/6-31+G* CPCM (dichloroethane). Fig. 7 summarizes the results from this computational investigation, the key findings of which are as follows – (a) regardless of the nature of the carbonyl and olefin substitution, the reaction proceeds via stepwise formation of the oxetane intermediate followed by a concerted asynchronous cycloreversion step (we located $\mathbf{TS_{C\text{-}C}}$, $\mathbf{TS_{C\text{-}O}}$, and $\mathbf{TS_{Rev}}$ for all four substrates); (b) for all substrates except **4**, $\mathbf{TS_{C\text{-}C}}$ and $\mathbf{TS_{C\text{-}O}}$ are within 1.5 kcal/mol, suggesting that the two steps have partial turnover-limiting influence; (c) for all substrates except **5**, $\mathbf{TS_{C\text{-}C}}$ has a lower $\Delta G^{\ddagger}$ (relative to the reactant-$FeCl_3$ complex) than $\mathbf{TS_{C\text{-}O}}$, and (d) cycloreversion is facile in all four reactions. Intrinsic reaction coordinate (IRC) calculations performed on $\mathbf{TS_{C\text{-}O}}$ (identical to the 'concerted' TS in ref. 6) lead to the oxetane intermediate in the forward direction and the betaine intermediate in the reverse direction, suggesting that this TS corresponds to the second step in the stepwise mechanism for oxetane formation and *not* a concerted asynchronous TS as proposed in ref. 6.

Discussion

In conclusion, using a combination of experimental ^{13}C KIE measurements, DFT evaluation of the reaction coordinate, AIMD metadynamics in solvent, and quasiclassical dynamic trajectories we have illustrated that the $FeCl_3$ catalyzed ring-closing COM to form polycyclic aromatic compounds proceeds via a stepwise mechanism for the formation of the oxetane intermediate followed by concerted cycloreversion to deliver the COM product. The turnover-limiting step in the catalytic cycle for the styrenyl-ketone reactant **5** is the formation of a betaine **8** (via $\mathbf{TS_{C\text{-}C}}$), which undergoes rapid C-O bond-forming ring-closure (via $\mathbf{TS_{C\text{-}O}}$) to generate the key oxetane intermediate. This result is at variance with the concerted asynchronous [2+2] cycloaddition mechanism for oxetane formation in this reaction proposed by Schindler and co-workers. We are currently investigating the generality of this stepwise oxetane-forming mechanism for other systems.

Methods

Synthesis of substrate 5

(*E*)-1-(2′-Styryl-[1,1′-biphenyl]-2-yl)ethanone (**5**) was prepared by Horner–Wadsworth–Emmons olefination of 2-bromobenzaldehyde with diethyl benzylphosphonate (NaH, THF), followed by Suzuki–Miyaura coupling of the resulting (*E*)-1-bromo-2-styrylbenzene with 2-acetylphenylboronic acid ($Pd(PPh_3)_4$, K_2CO_3, toluene/ethanol, 80 °C). The *E* isomer was obtained by crystallization. Full procedures and characterization data are given in Supplementary Notes 1 and 2.

Measurement of ^{13}C KIEs

$FeCl_3$ (0.3 mol%) was placed in a flask under nitrogen, and a solution of **5** (10.5 mmol) in dry 1,2-dichloroethane (0.1 M) was added. The mixture was stirred at room temperature and monitored by NMR. The reactions were stopped at 72.0%, 69.5% and 73.3% conversion in three independent experiments. Unreacted **5** was recovered by filtration through silica followed by column chromatography (hexane). The ^{13}C isotopic composition of each recovered sample was compared with that of an independent standard sample of **5** not subjected to the reaction, by quantitative ^{13}C NMR spectroscopy at 600 MHz. Relaxation delays were at least seven times the T_1 of the slowest-relaxing carbon. Six spectra were recorded for each sample. Peaks were integrated over a constant range equal to ten times the average peak width at half-height. KIEs were calculated from KIE = $\ln(1 - F)/\ln[(1 - F)R/R_0]$, where F is the fractional conversion and R/R_0 is the ratio of the ^{13}C composition of recovered **5** to that of the standard, relative to an internal standard carbon assumed to have a KIE of unity.[12] Isotope effects were calculated for each pair of measurements and averaged. Standard deviations and 95% confidence ranges (from the 18 individual isotope effects) are given in Supplementary Note 3 and Supplementary Table 1.

Ab initio molecular dynamics and metadynamics

Born–Oppenheimer AIMD simulations were performed with the QUICKSTEP module of CP2K 7.1[14] using the PBE functional,[15] DZVP basis sets with GTH pseudopotentials,[16] a 280 Ry plane-wave cutoff and the D3 dispersion correction.[17] The periodic cubic cell (25.0 Å) contained **5-$FeCl_3$** and 50 dichloroethane molecules. The SCF convergence criterion was 10^{-6} Hartree, the time step 0.5 fs, and the temperature (298 K) was controlled with a Nosé–Hoover thermostat (time constant 0.1 ps). After 3 ps of equilibration with the C1, C2, C3 and O positions constrained, sampling was enhanced by adding Gaussian hills (height 0.6 kcal mol^{-1}, width 0.1)

every 50 MD steps along two coordination-number collective variables, CV1 (C1–C2, d_0 = 2.8 Å) and CV2 (C3–O, d_0 = 3.0 Å). The free-energy surface was reconstructed with the graph.psmp utility of CP2K. Equivalent simulations were run without explicit solvent.

DFT calculations

Static DFT calculations were performed with Gaussian 16, Revision C.01.[23] Geometries were optimized at the B3LYP-D3(BJ)/6-31+G* level[17,30,34] with the CPCM solvent model for dichloroethane.[21,22] Minima had no imaginary frequencies, and transition structures had exactly one. Each transition structure was connected to its minima by IRC and QRC calculations. Gibbs free energies at 298.15 K include Grimme's quasi-rigid-rotor harmonic-oscillator correction.[24,25] Single-point energies were refined at the B3LYP-D3(BJ)/6-311++G** CPCM level. The functional dependence was examined by repeating the calculations with M06, M06-2X,[31] ωB97X-D,[32] PBE-D3(BJ)[15] and B97D[33] with the 6-31+G** basis set,[34] and with the def2-SVP basis set[35] for all atoms, including iron.

KIE predictions

^{13}C KIEs were predicted from scaled harmonic frequencies with the Bigeleisen–Mayer equation[26,28] as implemented in PyQuiver,[27] including a Wigner tunnelling correction.[29] Predicted KIEs were normalized to the carbon used as the internal standard in the experiments. Energy-weighted KIEs were obtained by Boltzmann weighting of the KIEs for $\mathbf{TS_{C\text{-}C}}$ and $\mathbf{TS_{C\text{-}O}}$ according to their free-energy difference at 298 K.

Variational transition state theory

Canonical variational transition state theory (CVT) and small-curvature tunnelling (SCT) calculations for betaine formation were carried out on the B3LYP-D3(BJ)/6-31+G* CPCM

(dichloroethane) surface with Gaussrate, the interface between Polyrate[36] and Gaussian 16, using the reorientation of the dividing surface (RODS) algorithm.

Quasiclassical direct dynamics

Quasiclassical trajectories were computed with Singleton's progdyn program[37,38] at the B3LYP-D3(BJ)/6-31+G* CPCM (dichloroethane) level at 298.15 K, with zero-point energy included and a 1.0 fs Verlet time step. Trajectories were initiated from the region of $\mathbf{TS_{C\text{-}C}}$ and integrated forward and backward in time until either **9-FeCl$_3$** or **5-FeCl$_3$** was formed. Trajectories that fully formed the C–C bond (to below 1.6 Å) and returned to **5-FeCl$_3$** within 250 fs were classified as deep recrossing. Of 118 trajectories, 4 recrossed immediately and were excluded from the KIE weighting.

Data availability

The data supporting the findings of this study are available within the article and its Supplementary Information, which contains experimental procedures, NMR data for the KIE measurements, computational details and the energies of all computed structures. Cartesian coordinates of all computed structures are provided as Supplementary Data 1 (COM_xyz.zip). Movies of the metadynamics simulation and of representative quasiclassical trajectories are provided as Supplementary Movies 1–3.

Code availability

Calculations used CP2K 7.1, Gaussian 16, Polyrate/Gaussrate, PyQuiver and progdyn, which are available from their developers. Input files for the CP2K metadynamics, Gaussrate and progdyn calculations are provided in Supplementary Notes 13–15. The in-house Python script used to plot the metadynamics free-energy surface is available from the corresponding authors upon request.

References

1. Albright, H. *et al.* Carbonyl-Olefin Metathesis. *Chem. Rev.* **121**, 9359–9406 (2021).
2. Ludwig, J. R., Zimmerman, P. M., Gianino, J. B. & Schindler, C. S. Iron(III)-Catalysed Carbonyl–Olefin Metathesis. *Nature* **533**, 374–379 (2016).
3. Schindler, C. *et al.* Inadequacy of Continuum Solvation for Polar Reactions: Predicting the Mechanism of Carbonyl–Olefin Metathesis. Preprint at https://doi.org/10.26434/chemrxiv-2022-nnp81 (2022).
4. Ludwig, J. R. *et al.* Mechanistic Investigations of the Iron(III)-Catalyzed Carbonyl-Olefin Metathesis Reaction. *J. Am. Chem. Soc.* **139**, 10832–10842 (2017).
5. Albright, H. *et al.* Catalytic Carbonyl-Olefin Metathesis of Aliphatic Ketones: Iron(III) Homo-Dimers as Lewis Acidic Superelectrophiles. *J. Am. Chem. Soc.* **141**, 1690–1700 (2019).
6. Becker, M. R., Reid, J. P., Rykaczewski, K. & Schindler, C. S. Models for Understanding Divergent Reactivity in Lewis Acid-Catalyzed Transformations of Carbonyls and Olefins. *ACS Catal.* **10**, 4387–4397 (2020).
7. Hanson, C. S., Psaltakis, M. C., Cortes, J. J. & Devery, J. J. Catalyst Behavior in Metal-Catalyzed Carbonyl-Olefin Metathesis. *J. Am. Chem. Soc.* **141**, 11870–11880 (2019).
8. Tran, U. P. N., Oss, G., Pace, D. P., Ho, J. & Nguyen, T. V. Tropylium-Promoted Carbonyl–Olefin Metathesis Reactions. *Chem. Sci.* **9**, 5145–5151 (2018).
9. Tran, U. P. N. *et al.* Carbonyl–Olefin Metathesis Catalyzed by Molecular Iodine. *ACS Catal.* **9**, 912–919 (2019).

10. Anh To, T., Pei, C., Koenigs, R. M. & Vinh Nguyen, T. Hydrogen Bonding Networks Enable Brønsted Acid-Catalyzed Carbonyl-Olefin Metathesis. *Angew. Chem. Int. Ed.* **61**, e202117366 (2022).
11. Djurovic, A. *et al.* Synthesis of Medium-Sized Carbocycles by Gallium-Catalyzed Tandem Carbonyl–Olefin Metathesis/Transfer Hydrogenation. *Org. Lett.* **21**, 8132–8137 (2019).
12. Singleton, D. A. & Thomas, A. A. High-Precision Simultaneous Determination of Multiple Small Kinetic Isotope Effects at Natural Abundance. *J. Am. Chem. Soc.* **117**, 9357–9358 (1995).
13. McAtee, C. C., Riehl, P. S. & Schindler, C. S. Polycyclic Aromatic Hydrocarbons via Iron(III)-Catalyzed Carbonyl–Olefin Metathesis. *J. Am. Chem. Soc.* **139**, 2960–2963 (2017).
14. VandeVondele, J. *et al.* Quickstep: Fast and Accurate Density Functional Calculations Using a Mixed Gaussian and Plane Waves Approach. *Comput. Phys. Commun.* **167**, 103–128 (2005).
15. Perdew, J. P., Burke, K. & Ernzerhof, M. Generalized Gradient Approximation Made Simple. *Phys. Rev. Lett.* **77**, 3865–3868 (1996).
16. Goedecker, S., Teter, M. & Hutter, J. Separable Dual-Space Gaussian Pseudopotentials. *Phys. Rev. B* **54**, 1703–1710 (1996).
17. Grimme, S., Antony, J., Ehrlich, S. & Krieg, H. A Consistent and Accurate *Ab Initio* Parametrization of Density Functional Dispersion Correction (DFT-D) for the 94 Elements H-Pu. *J. Chem. Phys.* **132**, 154104 (2010).

18. Fu, Y., Bernasconi, L. & Liu, P. Ab Initio Molecular Dynamics Simulations of the S_N1/S_N2 Mechanistic Continuum in Glycosylation Reactions. *J. Am. Chem. Soc.* **143**, 1577–1589 (2021).
19. Fu, Y. *et al.* Engineered P450 Atom-Transfer Radical Cyclases Are Bifunctional Biocatalysts: Reaction Mechanism and Origin of Enantioselectivity. *J. Am. Chem. Soc.* **144**, 13344–13355 (2022).
20. Peltzer, R. M., Gauss, J., Eisenstein, O. & Cascella, M. The Grignard Reaction – Unraveling a Chemical Puzzle. *J. Am. Chem. Soc.* **142**, 2984–2994 (2020).
21. Barone, V. & Cossi, M. Quantum Calculation of Molecular Energies and Energy Gradients in Solution by a Conductor Solvent Model. *J. Phys. Chem. A* **102**, 1995–2001 (1998).
22. Cossi, M., Rega, N., Scalmani, G. & Barone, V. Energies, Structures, and Electronic Properties of Molecules in Solution with the C-PCM Solvation Model. *J. Comput. Chem.* **24**, 669–681 (2003).
23. Frisch, M. J. *et al. Gaussian 16, Revision C.01* (Gaussian, Inc., 2016).
24. Grimme, S. Supramolecular Binding Thermodynamics by Dispersion-Corrected Density Functional Theory. *Chem. Eur. J.* **18**, 9955–9964 (2012).
25. Ribeiro, R. F., Marenich, A. V., Cramer, C. J. & Truhlar, D. G. Use of Solution-Phase Vibrational Frequencies in Continuum Models for the Free Energy of Solvation. *J. Phys. Chem. B* **115**, 14556–14562 (2011).
26. Bigeleisen, J. & Mayer, M. G. Calculation of Equilibrium Constants for Isotopic Exchange Reactions. *J. Chem. Phys.* **15**, 261–267 (1947).
27. Anderson, T. L. & Kwan, E. E. *PyQuiver* (2020); https://github.com/ekwan/PyQuiver.

28. Saunders, M., Laidig, K. E. & Wolfsberg, M. Theoretical Calculation of Equilibrium Isotope Effects Using Ab Initio Force Constants: Application to NMR Isotope Perturbation Studies. *J. Am. Chem. Soc.* **111**, 8989–8994 (1989).

29. Bell, R. P. *The Tunnel Effect in Chemistry* (Chapman and Hall, 1980).

30. Becke, A. D. Density-Functional Thermochemistry. III. The Role of Exact Exchange. *J. Chem. Phys.* **98**, 5648–5652 (1993).

31. Zhao, Y. & Truhlar, D. G. The M06 Suite of Density Functionals for Main Group Thermochemistry, Thermochemical Kinetics, Noncovalent Interactions, Excited States, and Transition Elements: Two New Functionals and Systematic Testing of Four M06-Class Functionals and 12 Other Functionals. *Theor. Chem. Acc.* **120**, 215–241 (2008).

32. Mardirossian, N. & Head-Gordon, M. ωB97X-V: A 10-Parameter, Range-Separated Hybrid, Generalized Gradient Approximation Density Functional with Nonlocal Correlation, Designed by a Survival-of-the-Fittest Strategy. *Phys. Chem. Chem. Phys.* **16**, 9904 (2014).

33. Grimme, S. Semiempirical GGA-type Density Functional Constructed with a Long-range Dispersion Correction. *J. Comput. Chem.* **27**, 1787–1799 (2006).

34. Hehre, W. J., Stewart, R. F. & Pople, J. A. Self-Consistent Molecular-Orbital Methods. I. Use of Gaussian Expansions of Slater-Type Atomic Orbitals. *J. Chem. Phys.* **51**, 2657–2664 (1969).

35. Weigend, F. & Ahlrichs, R. Balanced Basis Sets of Split Valence, Triple Zeta Valence and Quadruple Zeta Valence Quality for H to Rn: Design and Assessment of Accuracy. *Phys. Chem. Chem. Phys.* **7**, 3297 (2005).

36. Meana-Pañeda, R. *et al.* Polyrate 2023: A Computer Program for the Calculation of Chemical Reaction Rates for Polyatomics. New Version Announcement. *Comput. Phys. Commun.* **294**, 108933 (2024).

37. Gonzalez-James, O. M., Kwan, E. E. & Singleton, D. A. Entropic Intermediates and Hidden Rate-Limiting Steps in Seemingly Concerted Cycloadditions. Observation, Prediction, and Origin of an Isotope Effect on Recrossing. *J. Am. Chem. Soc.* **134**, 1914–1917 (2012).

38. Chen, Z., Nieves-Quinones, Y., Waas, J. R. & Singleton, D. A. Isotope Effects, Dynamic Matching, and Solvent Dynamics in a Wittig Reaction. Betaines as Bypassed Intermediates. *J. Am. Chem. Soc.* **136**, 13122–13125 (2014).

Acknowledgements

Research reported in this publication was supported by the National Institutes of Health (NIGMS) under R35 GM145320 (M.J.V.) and R35 GM147183 (J.S.H.); this support is gratefully acknowledged. Research reported in this publication was supported by the Office of The Director of the National Institutes of Health under Award Number S10OD026746. Computational support was provided through the ACCESS program, which is supported by National Science Foundation grants #2138259, #2138286, #2138307, #2137603, #2138296, utilizing allocations CHE180061 (J.S.H) and CHE160009 (M.J.V.).

Author contributions

T.D. and C.J. performed computations and A.D. and M.A.N. performed the experiments; M.J.V. and J.S.H. conceived and supervised the project and wrote the manuscript with input from all authors.

Competing interests

The authors declare no competing interests.

Supplementary Files

This is a list of supplementary files associated with this preprint. Click to download.

- COMNatCommSIFINAL.pdf
- MovieS2progdynrecross.mp4
- MovieS1AIMDmetadyn.mp4
- MovieS3progdynproductive.mp4
- COMxyz.zip
- COMNatCommSupplementaryFiles10132026.docx